Journal of Future Artificial Intelligence and Technologies

E-ISSN: 3048-3719

Research Article

Fusion of Wheel Encoded Data and RFID Signals using Kalman Filter for Robot Indoor Localization

Mui D. Nguyen [1], Thang C. Vu [2], Vu T. Hoang [2], Dung T. Nguyen [2], Tao V. Nguyen [2], Long Q. Dinh [2], Son Q. Tran [1], Vinh Q. Tran [3], and Minh T. Nguyen [1,*]

[1] Faculty of International Training, Thai Nguyen University of Technology, Thai Nguyen 24000, Viet Nam; e-mail: ducmui@tnut.edu.vn; tranqueson.ktdt@tnut.edu.vn; nguyentuanminh@tnut.edu.vn.
[2] Faculty of Engineering and Technology, Thai Nguyen University of Information and Communication Technology, Thai Nguyen 24000, Viet Nam; e-mail: vcthang@ictu.edu.vn; vuht.hgg@vnpt.vn; ntdungcndt@ictu.edu.vn; nvtao@ictu.edu.vn; dqlong@ictu.edu.vn.
[3] Department of communication engineering, School of Electrical and Electronic Engineering, Hanoi University of Science and Technology, Ha Noi 10000, Viet Nam; e-mail: vinh.tranquang1@hust.edu.vn.
* Corresponding Author: Minh T. Nguyen

Abstract: Indoor positioning technology plays an important role in improving efficiency and automating industrial processes such as warehouse management, production lines, and mobile robot navigation. However, existing RFID-based and odometry-only localization methods still suffer from limited accuracy, drift, and dependence on predefined infrastructure. To address these challenges, this work proposes a lightweight sensor fusion framework that combines wheel encoder data and phase-based RFID signals using an Extended Kalman Filter (EKF) for accurate indoor localization of mobile robots. The proposed method does not require prior knowledge of the tag map and enables convergence even when the robot starts outside the reader's range. Simulation results demonstrate that the fused method achieves an average positioning error of 5.4 cm and a final error of less than 8 cm. An ablation study comparing odometry-only, RFID-only, and fusion scenarios confirms the superiority of the integrated approach in terms of accuracy and robustness. The system is suitable for real-time implementation in cost-effective embedded platforms and has potential for deployment in smart warehouses and logistics environments.

Keywords: Extended Kalman Filter; Indoor Localization; Mobile Robot; RFID; Sensor Fusion.

Received: June, 25th 2025
Revised: July, 11th 2025
Accepted: July, 21st 2025
Published: July, 22nd 2025
Curr. Ver.: August, 20th 2025

1. Introduction

Indoor positioning has added new features to various industrial IoT applications, including production lines, warehousing, and mobile device navigation. The rapid acquisition of location information of objects will improve the efficiency of industrial processes, providing users with timely information and other services. The most common indoor positioning techniques can be classified into the following categories: computer vision-based, inertial navigation-based, wireless communication infrastructure-based (e.g., WiFi, 4G/5G), dedicated wireless communication (e.g., Bluetooth, ZigBee, Infrared), and radio frequency identification (RFID). Due to the advantages of system simplicity and no line of sight (NLoS), wireless infrastructure-based positioning and radio frequency-based positioning are gaining increasing attention [1]–[7].

However, existing RFID-based positioning systems still face several limitations. First, RSSI-based approaches suffer from high variability due to multipath and environmental interference, leading to unreliable estimates [8]. Second, phase-based RFID localization methods require complex antenna arrays or precise tag layouts to achieve acceptable accuracy [9]. Similarly, odometry-only localization methods are prone to cumulative drift over time due to wheel slip and the lack of external corrections [10]. SLAM-based methods using RFID often rely on predefined tag maps or large computational resources, which limits their practicality

in dynamic or unknown environments [11]. To overcome these limitations, our work proposes a lightweight fusion framework using an Extended Kalman Filter (EKF) that combines RFID phase data and encoder odometry to estimate both the robot's pose and target location, even when the robot starts outside the RFID reader range. Unlike previous works, our approach does not require prior tag layouts or expensive antenna arrays and can robustly navigate toward the target using minimal infrastructure. Furthermore, this work builds on recent advances in hybrid RFID localization [12], real-time RFID-based SLAM [13], and multi-sensor fusion for mobile robots [14], thereby positioning our method as a practical and scalable solution for real-world robot navigation in indoor environments.

This demand is particularly urgent in high-throughput environments such as Amazon warehouses, where Autonomous Guided Vehicles (AGVs) must navigate complex aisles to pick and deliver items with sub-decimeter accuracy. Similarly, in logistics centers and smart factories, mobile robots are increasingly utilized for pick-and-place operations, shelf inventory scanning, and product delivery, where precise localization is essential for ensuring safety, facilitating task coordination, and preventing collisions. These scenarios demand robust, infrastructure-light, and real-time localization methods that can work reliably even in cluttered, multipath-prone indoor spaces where GPS is unavailable.

Simultaneous acquisition of both location and ID information is expected for autonomous operation and data integration. Therefore, RFID technology with unique ID identification will be more competitive. In addition, RFID achieves identification through NLoS wireless transmission and simultaneously reads multiple tags [15]–[21]. When attached to the surface of an object inside a package, it can be retrieved by the RF backscatter technique to read and locate the ID. This is superior to other positioning devices in its ability to integrate identification and positioning [22]. Due to the advantages of simultaneous identification and positioning, RFID-based techniques have attracted wide attention in both academia and industry. Positioning accuracy is affected by various parameters, including the transmitting and receiving antennas, as well as the surrounding environment of RFID tags [23]. RF signal parameters related to positioning may include received signal strength index (RSSI), time of arrival (ToA), and phase shift [24]. From the perspective of the object to be tracked, it can refer to techniques for locating stationary objects and moving objects, such as robots. The positioning results can be classified into absolute position and relative position [25]–[27]. In [28], a robot positioning solution using RFID was described. The reader is mounted on the robot, and the tags are fixed on the ceiling. The received signal strength index (RSSI) and the phase difference of the UHF-RFID signal are used to determine the robot's position. However, the requirement is to know the layout of the RFID tags in advance, and since the tags are passive, the power supply needed for the tag to operate must be noted. Another study combines the RSSI index and the link quality index (LQI) to determine the robot's position [29]. The signal strength distribution map is created, and the signal strengths of the transmitter and receiver are compared. The study did not address or resolve the issue of the robot operating outside the RFID range.

Another solution is to perform RFID-based simultaneous localization and mapping (RF-SLAM), as presented in [13]. RF-SLAM converts RFID measurements into relative tag position constraints and uses the corresponding graph model to perform SLAM. Phase antennas and short-term distance measurement data are utilized as part of the end-to-end solution. Although this solution requires larger computational resources, it allows positioning in 3D environments with an accuracy of about 5-10 cm. Research [30] aims to address the issue of inconsistent robot speeds when locating them using RFID. A lightweight algorithm optimally utilizes the data to calculate positions in 2D and 3D space. In which the characteristics of the distance between tags and antennas are combined with phase data from multiple antennas to eliminate the unwanted effects of inconsistent velocity.

The potential of RFID positioning is immense, but a gap still exists between research and practical application [31]. Moreover, recent studies such as [32] emphasize the importance of addressing path planning challenges as key aspects of deploying mobile robots in dynamic environments. This work involves positioning an object attached to a reader, and the estimation of the object's position begins when the robot enters the operating range of the tag. The ability to move towards the target of the tagged robot is achieved using a Kalman filter [33], which combines the robot's distance measurement data [34] with the phase difference of the RFID signal.

The rest of this work is organized as follows. Section 2 introduces the kinematic model of the differential-drive robot and details the Extended Kalman Filter-based localization framework. Section 3 presents the simulation setup, performance analysis, ablation studies, and comparative evaluations with existing methods. Finally, Part 4 concludes and discusses some further research directions.

2. Kinematic Model of Mobile Robot and Robot Position Estimation

The simulation uses a mobile robot equipped with an RFID reader. To conduct the simulation, a robot model was developed and built to include the measurements received from the wheel encoder and the signals measured by the reader.

2.1. Differential Drive Robot Kinematic Model

The agent used in the paper is selected as a mobile robot based on the differential drive model. The geometry and kinematic parameters of TWMR are shown in Figure 1.

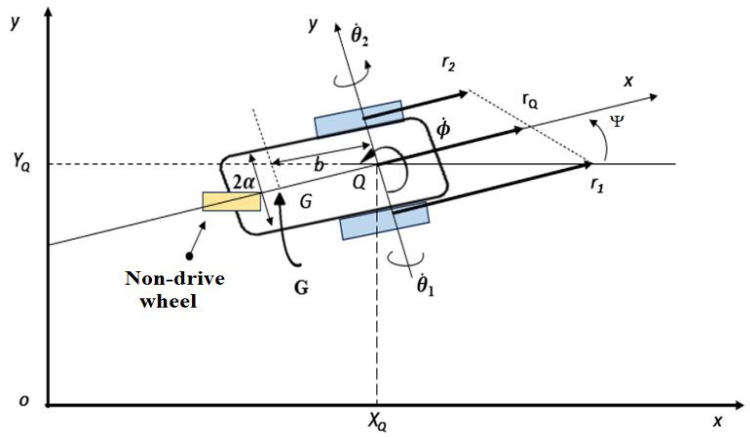

Figure 1. Mobile robot TWMR geometry and kinematic parameters

The posture vector (position/orientation) of the WMR (wheeled mobile robot) and its speed are respectively:

$$q = \begin{bmatrix} x_Q \\ y_Q \\ \phi \end{bmatrix}, \dot{q} = \begin{bmatrix} \dot{x}_Q \\ \dot{y}_Q \\ \dot{\phi} \end{bmatrix} \tag{1}$$

Suppose v_l and v_r are the linear velocities of the left and right wheels, respectively, and v is the velocity of the center point of wheel v_Q of TWMR. Then, from Figure 1 we have:

$$v_r = v_Q + a\dot{\theta}, v_l = v_Q - a\dot{\theta} \tag{2}$$

Add and subtract v_r and v_l, we have

$$v_Q = 0.5(v_\mathrm{r} + v_\mathrm{l}), \qquad 2a\dot{\theta} = 2a\omega = v_\mathrm{r} - v_\mathrm{l} \tag{3}$$

We have $v_\mathrm{r} = r\dot{\theta}_\mathrm{r}$ and $v_\mathrm{l} = r\dot{\theta}_\mathrm{l}$, where r is the radius of the robot wheel. The kinematic model can be obtained by expressing the TWMR velocity in terms of the linear velocity and angular velocity of the TWMR in the robot frame as follows.

$$\dot{p} = \begin{bmatrix} \dot{x}_Q \\ \dot{y}_Q \\ \dot{\theta} \end{bmatrix} = \begin{bmatrix} cos(\theta) & 0 \\ sin(\theta) & 0 \\ 0 & 1 \end{bmatrix} \begin{bmatrix} v \\ w \end{bmatrix} \tag{4}$$

and non-global constraints

$$-\dot{x}_Q sin\phi + \dot{y}_Q cos\phi = 0 \tag{5}$$

2.2 Robot Odometry Model

To conduct the simulation, the Euler method is used to decompose the internal systems, resulting in:

$$\begin{aligned} x_{k+1} &= x_k + v_k\, cos(\theta_k)\Delta t, \\ y_{k+1} &= y_k + v_k\, sin(\theta_k)\Delta t, \\ \theta_{k+1} &= \theta_k + \omega\Delta t \end{aligned} \tag{6}$$

where Δt is the integration step. The robot encoder readings are related to wheel displacement, so the robot system measurement is modeled as follows:

$$\hat{u}_R = u_R + \eta_R\ \hat{u}_R = u_R + \eta_R \tag{7}$$

where the noise is a Gaussian random variable with variance:

$$\sigma_R^2 = K_R|u_R|\ \sigma_L^2 = K_L|u_L| \tag{8}$$

The variance is calculated as the value proportional to the actual displacement divided by the constant coefficients K_R and K_L. This model of the measurement system was used in the development of the distance measurement model. An approximation for the wheel speed can be derived as in Equation (9).

$$\omega_R = \frac{d}{dt}\phi_R \simeq \frac{\Delta\phi_R}{\Delta t}\ \omega_R = \frac{d}{dt}\phi_R \simeq \frac{\Delta\phi_R}{\Delta t} \tag{9}$$

where $\Delta\phi_R, \Delta\phi_L$ are the angular displacements of the wheels. Substituting Equation (9) into the discrete model described in Equation 6, the resulting system can be expressed as follows.

$$\begin{aligned} x_{k+1} &= x_k + \frac{R}{2}(\Delta\phi_R + \Delta\phi_L)cos(\theta_k) \\ y_{k+1} &= y_k + \frac{R}{2}(\Delta\phi_R + \Delta\phi_L)sin(\theta_k) \\ \theta_{k+1} &= \theta_k + \frac{R}{d}(\Delta\phi_R + \Delta\phi_L) \end{aligned} \tag{10}$$

The displacement of the wheel can be written as:

$$u_L = R\Delta\phi_L\ u_R = R\Delta\phi_R \tag{11}$$

Considering the measurements of the quantities describing the position, the distance estimation model is:

$$\begin{aligned} \hat{x}_{k+1} &= \hat{x}_k + \frac{1}{2}\left(\hat{u}_{R,k} + \hat{u}_{L,k}\right)cos(\theta_k) \\ \hat{y}_{k+1} &= \hat{y}_k + \frac{1}{2}\left(\hat{u}_{R,k} + \hat{u}_{L,k}\right)sin(\theta_k) \\ \theta_{k+1} &= \hat{\theta}_k + \frac{1}{d}\left(\hat{u}_{R,k} - \hat{u}_{L,k}\right) \end{aligned} \tag{12}$$

To keep it simple, set $\hat{u}_k = \frac{\hat{u}_{R,k}+\hat{u}_{L,k}}{2}\ \hat{\omega}_k = \frac{\hat{u}_{R,k}-\hat{u}_{L,k}}{d}$.
The final pose estimation of the robot can be seen as described in Equation (13).

$$\hat{x}_{k+1} = \hat{x}_k + \hat{u}_k cos\ (\theta_k)\ \hat{y}_{k+1} = \hat{y}_k + \hat{u}_k sin\ (\theta_k)\ \theta_{k+1} = \hat{\theta}_k + \hat{\omega}_k \tag{13}$$

2.3. RFID Model

Radio Frequency Identification (RFID) is a technology that uses radio waves to transmit data between two main components: RFID tags and RFID readers. Readers have antennas that emit radio frequency signals, while tags have antennas that are responsible for receiving and retransmitting these signals. Typically, the tags are passive and only activate when they receive a signal from the reader.

When a tag enters the reader's range, the reader sends a signal. The tag, upon receiving the signal, is powered by the energy from the incoming radio waves. The powered tag then transmits it back to the reader. The reader receives the signal and can measure the phase

difference between the signal sent and received. For a signal of frequency f, the phase of this signal over time is calculated as follows:

$$\varphi = \omega \cdot t \text{ , where } \omega = 2\pi f \tag{14}$$

In this project, the phase measurement model at time step k is considered as follows:

$$\varphi = mod\left(-\frac{4\pi}{\lambda} \cdot \rho_k + \eta_{\varphi,k}, 2\pi\right) \tag{15}$$

where λ is the wavelength of the electromagnetic signal, ρ_k is the unknown tag-to-reader distance, and η_φ is the average Gaussian noise, i.e. $\eta_\varphi \sim N(0, \sigma_\varphi^2)$. Assuming the signal travels from reader to tag and back, the distance between them will be:

$$d = \frac{1}{2} c \cdot t_f \tag{16}$$

where c is the speed of light and t_f is the time of flight. Therefore, the distance between the tag and the reader can be expressed as:

$$d = \frac{1}{2} c \frac{\varphi}{\omega} = \frac{1}{2} \frac{c\varphi}{2\pi f} = \frac{1}{2} \frac{\lambda}{2\pi} (2n\pi + \varphi) \tag{17}$$

The main challenge encountered is that the reader can only measure φ, which makes it impossible to obtain the number of wavelengths (n) directly. This limitation therefore makes it difficult to determine the distance between the tag and the reader accurately.

2.4. Locate Tags with EKF Filter

The robot tag distance ρ and the azimuth angle β are two parameters used to determine the tag position relative to the robot position.

$$\rho = \sqrt{(x_r - x_T)^2 + (y_r - y_T)^2} \tag{18}$$

$$\beta = \theta_r - atan2(y_T - y_r, x_T - x_r) \tag{19}$$

After discretization, the dynamics of the variables ρ_k and β_k are expressed as functions of the wheel displacements $u_{R,k}$ and $u_{L,k}$.

$$\rho_{k+1} = \rho_k - u_k \, cos \, cos \, (\beta_k) \tag{20}$$

$$\beta_{k+1} = \beta_k + \omega_k(\beta_k) \tag{21}$$

The goal is to retrieve the tag location using simple encoded reading and RFID signal phase measurement. A proposed solution is to implement a Kalman Filter to estimate the system state directly $\xi = (\rho_k \; \beta_k \; x_k \; y_k \; \theta_k)^T$ of the problem. The measurement model is:

$$z_k = (1\;0\;0\;0\;0\;)\xi + \eta_k \tag{22}$$

Assuming the maximum range ρ_{max} over which the reader can detect the tag is known, each phase measurement can correspond to one of $n_{max} = \frac{\rho_{max}}{\lambda/2}$ different possible distances between the robot and the tag. Therefore, several Kalman filters are used to evaluate all these different hypotheses. The steps represent the procedure for the EKF.

1) Initialization: The filter is initialized as soon as the phase measurement is available. Suppose the initial state of the EKF is as follows:

$$\hat{\rho}_0 = -\frac{1}{4\pi}\lambda\hat{\varphi} + n\frac{\lambda}{2} \;\; n = 1, \ldots, n_{max} \tag{23}$$

$$\hat{\beta} = 0 \tag{24}$$

$$\hat{x}_0 = x_i \tag{25}$$

$$\hat{y}_0 = y_i \tag{26}$$

$$\hat{\theta}_0 = \theta_i \tag{27}$$

$$\hat{\theta}_0 = \theta_i \tag{27}$$

and the initial covariance matrix of the estimate as

$$P_0 = \begin{pmatrix} \sigma_\varphi^2 & 0 & 0 & 0 & 0 \\ 0 & (\pi/3)^2 & 0 & 0 & 0 \\ 0 & 0 & cov(x_i^2) & cov(x_i y_i) & cov(x_i \theta_i) \\ 0 & 0 & cov(y_i x_i) & cov(y_i^2) & cov(y_i \theta_i) \\ 0 & 0 & cov(\theta_i x_i) & cov(\theta_i y_i) & cov(\theta_i^2) \end{pmatrix} \tag{28}$$

2) Prediction steps are:

$$\hat{\rho}_{k+1}^- = \hat{\rho}_k - \hat{u}_k \, cos \, cos \, (\beta_k) \tag{29}$$

$$\hat{\beta}_{k+1}^- = \hat{\beta}_k + \hat{\omega}_k + \frac{\hat{u}_k}{\rho_k} sin \, sin \, (\beta_k) \tag{30}$$

$$\hat{x}_{k+1}^- = \hat{x}_k + \frac{1}{2} cos \, \hat{u}_k cos \, (\theta_k) \tag{31}$$

$$\hat{y}_{k+1}^- = \hat{y}_k + \frac{1}{2} sin \, \hat{u}_k sin \, (\theta_k) \tag{32}$$

$$\hat{\theta}_{k+1}^- = \hat{\theta}_k + \frac{1}{d} \hat{\omega}_k \tag{33}$$

$$P_{k+1}^- = F_k P_k F_k^T + W_k Q_k W_k^T \tag{34}$$

3) Calibration step: Assuming $z_{k+1} = \varphi_{k+1} + \eta_\rho$ is the available measurement at time step $k+1$, the innovation rank is given by $\varphi_{k+1} - \hat{\varphi}_{k+1}$, where $\hat{\varphi}_{k+1} = mod(-\frac{4\pi}{\lambda} \cdot \hat{\rho}_{k+1}, 2\pi)$ is the expected phase measurement at this stage. Therefore, the correction step, for the state and covariance matrices, is:

$$\hat{\xi}_{k+1} = \hat{\xi}_{k+1}^- + K_{k+1}(\varphi_{k+1} - \hat{\varphi}_{k+1}) \tag{35}$$

$$P_{k+1} = (I - K_{k+1} H) \, P_{k+1}^- \tag{36}$$

$$K_{k+1} = P_{k+1}^- H^T (H \, P_{k+1}^- \, H^T + \sigma_\rho^2)^{-1} \tag{37}$$

is the Kalman gain, and the Jacobian matrix H is given by:

$$H = \left(-\frac{4\pi}{\lambda}, 0, 0, 0, 0 \right) \tag{38}$$

The EKF was chosen over alternatives such as the Unscented Kalman Filter (UKF) or Particle Filter due to a balance between computational efficiency and estimation accuracy. While UKF and Particle Filters are known for handling stronger non-linearities or multi-modal distributions, they often require significantly more computational resources and are more complex to tune. Since the motion and observation models in this work exhibit mild non-linearity, the EKF provides sufficient accuracy while maintaining low computational cost, as shown in subsection 3.4 with a real-time update rate of 244 Hz. This makes EKF more suitable for embedded implementations, especially for low-power AGVs or mobile

robots. Moreover, among RFID signal features, phase difference offers better distance resolution than RSSI, which is highly sensitive to environmental interference and multipath fading. Unlike RSSI, the phase shift contains deterministic correlation with path length in line-of-sight (LoS) settings, enabling more accurate ranging. By fusing odometry and RFID phase via EKF, the system can combine the short-term accuracy of wheel encoders with the global correction ability of RFID phase, enhancing robustness against drift and providing reliable convergence even from outside the reader's range. This hybrid approach leverages complementary strengths and has proven to reduce final position error to below 8 cm in our simulation results, as shown in subsection 3.3.

2.5. End-to-End System Flow Diagram

To further illustrate the positioning process, an end-to-end system flow diagram is provided in Figure 2. The diagram describes the main stages of the method, starting from sensing inputs to position estimation and movement toward the target: Wheel encoder readings are used to compute odometry; RFID reader measures the phase shift between transmitted and received signals; Both sources of data are fused within the EKF to estimate the robot's pose and distance to the tag; and The estimated position is used to guide the robot toward the target in successive update steps.

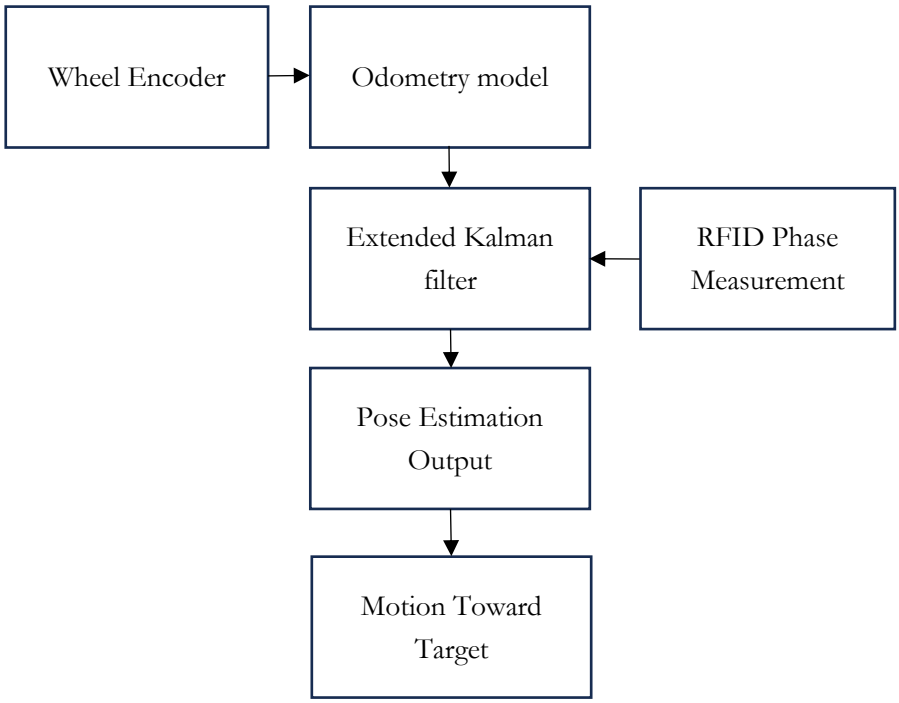

Figure 2. End-to-End system flow diagram of the proposed positioning method

3. Simulation Results

3.1. Simulation Configuration

The simulation was implemented in MATLAB and used the following parameters and assumptions: RFID Frequency at 915 MHz (UHF band), corresponding to a wavelength of approximately 0.328 m; Wheel Radius: 0.05 m; Wheelbase: 0.3 m; and Integration Time Step: 0.1 s. EKF Process Noise Covariance: $Q = diag([1e^{-4}, 1e^{-4}, 1e^{-6}])$ for x, y, θ. Measurement Noise Covariance: $R = diag([1e^{-2}, 1e^{-2}])$ for distance and angle; Initial Pose Estimate: Randomized outside reader range; Phase Noise: Modeled as Gaussian noise with a standard deviation of 0.05 rad; and RFID Model: Assumes line-of-sight (LoS) operation without multipath, environmental noise, and obstacles, which were not explicitly modeled in this version. Future work will investigate performance under multipath effects and dynamic environments with physical obstacles.

Table 1. Simulation Parameters

Parameter	Value	Description
RFID Frequency	915 MHz	UHF RFID band
Wavelength (λ)	~0.328 m	Derived from the RFID frequency
Wheel Radius	0.05 m	Radius of each wheel
Wheelbase	0.3 m	Distance between left and right wheels
Encoder Resolution	1024 pulses/rev	Resolution of wheel encoders (assumed)
Integration Time Step (Δt)	0.1 s	Discrete simulation interval
EKF Process Noise Covariance (Q)	diag([$1e^{-4}$, $1e^{-4}$, $1e^{-6}$])	For x, y, and heading angle
Measurement Noise Covariance (R)	diag([$1e^{-2}$, $1e^{-2}$])	For distance and azimuth angle
Phase Noise Std. Dev.	0.05 rad	Gaussian phase measurement noise
Initial Pose	Randomized outside a 2m range	The robot starts outside the reader's range
RFID Range	2 m	Operating radius of the reader

Table 1 serves as a reference for parameter values used in all simulation runs described in Subsection 3.2

3.2. Analysis of Estimation Results

The idea is to leverage the functionality of the Kalman Filter, merge the wheel encoder readings with the RFID signals, and then generate a certain number of EKF instances. Each instance is initialized on a different cycle corresponding to the initial phase measurement. Finally, one of these different instances is selected to estimate the distance between the robot and the tag. The robot will gradually move towards the reader's position, which is known in advance based on its position estimate.

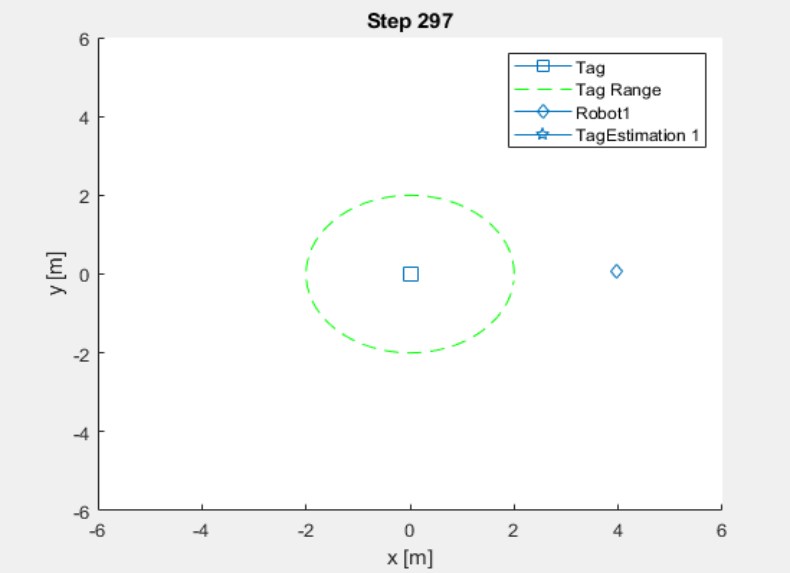

Figure 3. Set the initial position of the reader (Tag) and the RFID tagging robot

During the initial setup, as shown in Figure 3, the card reader (blue square) is positioned at the coordinates [0, 0] with a circular operating range of 2m radius (green dashed line). The robot (blue diamond) has an arbitrary initial position but is outside the scanning range of the reader. At the 297th estimation step, the positions of the objects are as shown in the figure above.

At the estimation step 569 shown in Figure 4, when the robot performs the estimation through communication between the tag and the reader, it begins to be within the operating range of the Tag reader, with a radius of 2m. An estimated result of the tag's location has appeared (blue star). The robot will consider this estimated Tag location as the target to move to. As can be seen, the estimated Tag location is relatively accurate compared to the actual location of the tag in the coordinate system.

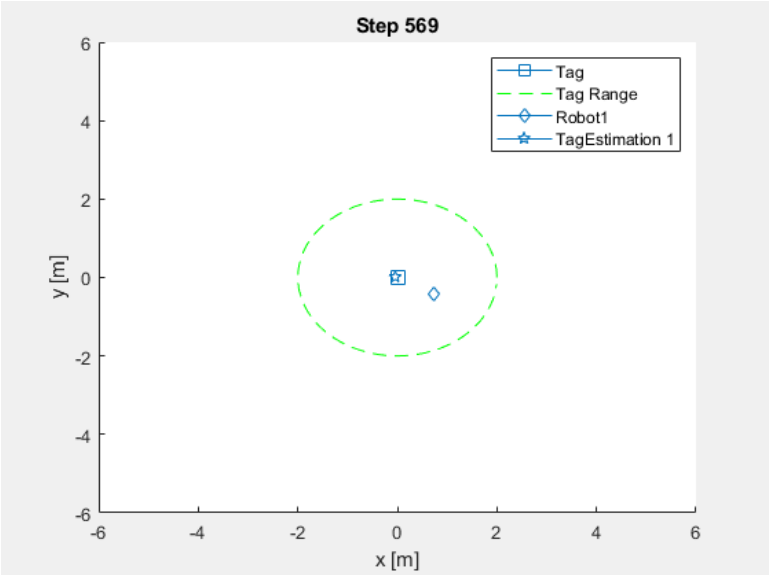

Figure 4. Object positions at estimation step 569

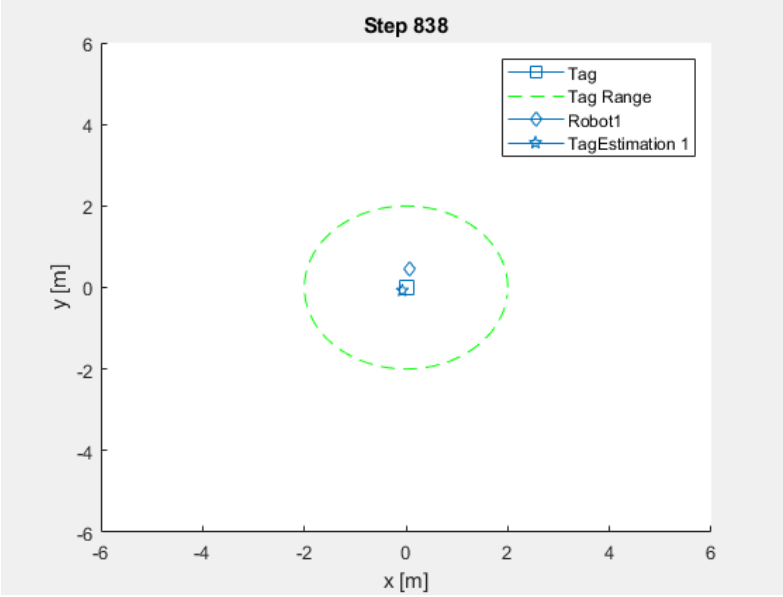

Figure 5. Location of objects at estimation step 838

At update step 838 shown in Figure 5, the robot has moved closer to the estimated position of the tag. Now through the update and estimation steps. The estimated position of the tag has a small change compared to the previous steps. But this deviation is still acceptable and still very close to the actual position of the reader.

At the estimation step 1168 shown in Figure 6, the RFID tag-carrying robot has come very close to the target, which is the reader. This indicates that the convergence speed of the Kalman filter when updating the robot's position and trajectory is excellent. At the same time, the new estimated position of the tag, compared to the actual position and previous positions, remains stable and changes only slightly.

The results show all the states of the robot from the start at position x = 2.29733 and y = 4.47681. The movement is performed by continuously updating the position and estimating the distance to the target using the tag reader. At the final update position (after 2500 update and estimation steps), the robot and the Tag reader have positions x = -0.0230681 and y = -0.0756305. The error is small compared to the actual position that needs to be performed, as the initial target is x, y = [0, 0]. This result describes the effectiveness of locating and navigating the robot to the target when using RFID positioning.

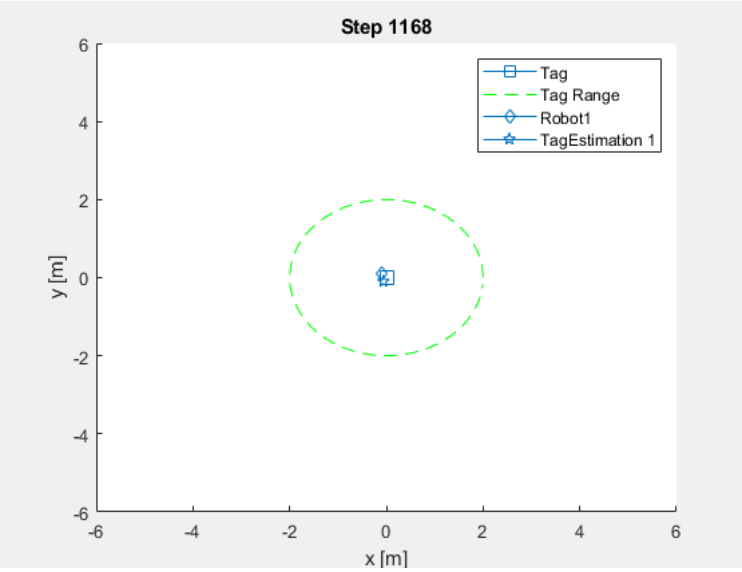

Figure 6. Object positions at estimation step 1168

At the estimation step 1168 shown in Figure 6, the RFID tag-carrying robot has come very close to the target, which is the reader. This shows that the convergence speed of the Kalman filter when updating the robot's position and trajectory is very good. At the same time, the new estimated position of the tag, compared to the actual position and previous positions, remains stable and changes only slightly.

The estimation results, including the robot's trajectory and final position relative to the RFID tag, are illustrated in Figure 7. The results show all the states of the robot from the start at position x = 2.29733 and y = 4.47681. The movement is performed by continuously updating the position and estimating the distance to the target using the tag reader. At the final update position (after 2500 update and estimation steps), the robot and the Tag reader have positions x = -0.0230681 and y = -0.0756305. The error is small compared to the actual position that needs to be performed, as the initial target is x, y = [0, 0]. This result describes the effectiveness of locating and navigating the robot to the target when using RFID positioning.

One critical challenge in using RFID for localization is its sensitivity to phase noise, which is caused by hardware instability, multipath reflections, and environmental interference. Even small fluctuations in measured phase can introduce distance estimation errors of several centimeters, especially when the tag-reader distance approaches integer multiples of the wavelength. The nλ ambiguity problem further complicates this issue by making the measured phase periodic, resulting in multiple valid hypotheses for tag distance. To address this, the system initializes multiple EKF instances with different phase offset assumptions and selects the one that converges consistently. While this strategy improves robustness, it increases computational load and requires reliable filter selection logic. Odometry data, despite its tendency to drift over time due to wheel slip or surface variation, provides smooth and continuous motion estimation. Its fusion with the RFID phase via EKF acts as a constraint and stabilizer, filtering out abrupt phase-induced deviations. However, in high-speed scenarios or environments with strong multipath effects, this approach may still suffer from temporary divergence or slower convergence. These insights highlight the trade-off between sensor accuracy, computation, and robustness, and justify further investigation into adaptive noise modeling, IMU integration, and phase-unwrapping algorithms in future work.

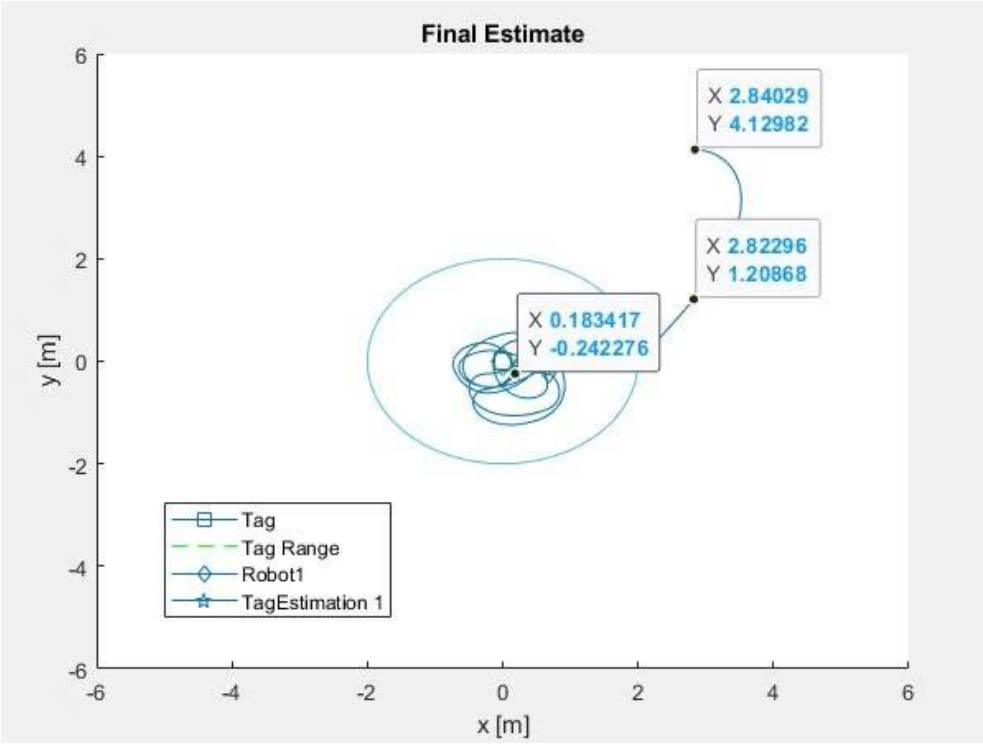

Figure 7. The tag synthesizes the robot's states when it moves, positions, and approaches the target tag.

3.3. Practical Interpretation of Results

The final positioning error after 2500 update steps was approximately 2.3 cm in x and 7.6 cm in y, resulting in a Euclidean distance error of roughly 7.9 cm. This level of accuracy is within the acceptable range for indoor navigation tasks. In typical warehouse environments, Automated Guided Vehicles (AGVs) are expected to operate with a positioning accuracy of less than 10 cm to ensure safe and efficient movement between racks, loading docks, and other structures [35]. Therefore, the simulation confirms that the proposed method, despite its low-cost and lightweight implementation, meets the precision demands for practical AGV deployments. Furthermore, the convergence behavior of the EKF, as demonstrated by the robot's progressive movement toward the estimated tag, illustrates the system's robustness under sensor fusion, even when starting outside the detection range.

3.4. Computational Performance and Real-Time Considerations

The simulation was executed on a standard laptop with an Intel Core i5-1135G7 CPU at 2.40 GHz and 8 GB RAM, using MATLAB R2023a. The average computation time per update step of the EKF, including prediction and correction using encoder and RFID phase data, was approximately 4.1 milliseconds, equivalent to a processing frequency of about 244 Hz. This latency is significantly below the typical control loop frequency of embedded robotic systems (for example, 10–100 Hz), indicating the method's feasibility for real-time deployment. In terms of computational resource usage, the proposed method maintains a low memory overhead, as the EKF state vector is compact and does not require storing large maps or particle clouds, unlike in SLAM methods. Even when multiple EKF instances are initialized to resolve phase ambiguity ($n\lambda$ problem), the number of filters remains small, typically less than 10, keeping total computation manageable. These results suggest that the algorithm can be implemented efficiently on embedded platforms, such as the Raspberry Pi 4, NVIDIA Jetson Nano, or STM32-based robots, for real-time AGV localization tasks in indoor environments.

3.5. Comparison of Localization Strategies

To evaluate the individual contributions of odometry and RFID, and to validate the effectiveness of combining them, we conducted a feature ablation study. This analysis helps

identify how each component impacts the system's overall positioning accuracy and robustness. The results of three different scenarios: (1) odometry-only: Robot position is estimated purely from encoder data using standard kinematic equations; (2) RFID-only: Robot localizes based on RFID phase measurements without odometry fusion; and (3) odometry + RFID (EKF fusion): Full system using EKF to fuse odometry and RFID data (proposed method). They are compared below to confirm the benefits of multi-sensor integration. Each scenario was run for 2500 steps with identical initial conditions and measurement noise.

The results in Table 2 clearly demonstrate that the EKF fusion of odometry and RFID significantly improves localization accuracy. The odometry-only approach suffers from accumulated drift, especially due to wheel slippage. The RFID-only method improves accuracy but lacks motion continuity and is sensitive to phase noise. The fusion method balances both, leveraging the short-term stability of encoders and the long-range correction capability of RFID, resulting in a robust and accurate localization system suitable for real-world indoor mobile robots. The table below shows the average and final positioning error in cm for each case as follows.

Table 2. Average and final positioning errors under different localization strategies.

Method	Average Error (cm)	Final Error (cm)
Odometry-only	16.7	28.2
RFID-only	12.3	15.9
Odometry + RFID (EKF)	5.4	7.9

For real-world deployment, the EKF algorithm should be executed at a control loop rate between 10–50 Hz, which aligns with the sensing and actuation cycle of most indoor mobile robots. The key required sensors include: Quadrature encoders on the drive wheels, providing real-time odometry; and an RFID reader compatible with UHF tags, capable of reporting phase values. The system can be deployed on low-cost embedded platforms such as Raspberry Pi 4, Jetson Nano, or STM32 MCUs, depending on power and real-time constraints. A lightweight embedded version of the EKF with fixed-size matrix operations can be implemented in C++ or Python using libraries like Eigen or OpenCV. For initial testing, the simulation code in MATLAB can be ported to ROS-based environments using ros_control, robot_localization, and rfid_driver packages. This enables integration with real sensors and robot operating systems.

4. Discussion

The simulation results validate the feasibility and effectiveness of the proposed RFID-based localization system in guiding a differential-drive mobile robot toward a predefined target location. By fusing wheel encoder readings with RFID phase measurements through the EKF, the system demonstrated the ability to maintain reliable localization, even when the robot initially started outside the RFID reader's detection range. The integration of multiple EKF instances effectively addressed the inherent challenge of resolving phase ambiguity, albeit with a trade-off in computational complexity.

The convergence behavior observed in the simulation confirmed that the EKF could correct the odometry drift by leveraging the global positioning reference provided by the RFID phase measurements. The final positioning error—approximately 7.9 cm after 2500 update steps—falls within acceptable bounds for industrial applications such as warehouse automation and AGV navigation, where sub-decimeter accuracy is often required. The complementary characteristics of odometry and RFID were evident: odometry offered smooth and continuous motion estimation but suffered from cumulative drift due to factors like wheel slippage, while RFID provided absolute positioning cues but was sensitive to phase noise, multipath interference, and measurement ambiguity.

Despite the advantages of combining wheel encoder data and RFID signals via an EKF, this approach also presents several inherent limitations. First, reliance on wheel odometry inherently exposes the system to drift errors caused by wheel slippage, especially on slippery or uneven surfaces. Second, the phase-based RFID distance estimation faces the classical $n\lambda$ ambiguity problem, where the actual distance between the tag and reader cannot be uniquely determined from a single-phase measurement due to its periodic nature. Although

this limitation was mitigated by initializing multiple EKF instances with different phase hypotheses, this strategy introduced additional computational overhead. Third, at high robot speeds, rapid positional changes may exceed the update rate of the RFID system, resulting in phase mismatches or delays in sensor fusion, and consequently reducing localization accuracy. These limitations highlight the trade-offs between sensor accuracy, computational efficiency, and robustness, emphasizing the need for future work to investigate advanced sensor fusion strategies, adaptive EKF tuning, and machine learning-based phase unwrapping algorithms for enhanced performance in dynamic and complex environments.

The discussion also highlights the potential benefits of integrating complementary sensor modalities, such as inertial measurement units (IMUs), LiDAR, or vision-based systems, to enhance localization robustness. These additional sensors could address the identified shortcomings, particularly in scenarios with high dynamic movement, multipath-prone environments, or non-line-of-sight conditions that compromise the integrity of RFID signals.

5. Conclusions and Future Work

This study successfully proposed and validated a sensor fusion framework for indoor localization of differential-drive mobile robots, combining wheel encoder odometry and RFID phase-based measurements using the EKF. The primary objective, which is to achieve accurate and robust robot localization without prior knowledge of RFID tag placement, was fully met through simulation experiments. The results demonstrated that the proposed approach can achieve sub-decimeter accuracy, maintain reliable convergence even when the robot starts outside the reader's range, and operate within the computational constraints of real-time embedded platforms. The significance of this work lies in its contribution to advancing lightweight and infrastructure-efficient localization methods suitable for practical applications, particularly in smart warehouses, logistics centers, and indoor robotic navigation systems. By eliminating the dependency on predefined tag maps and leveraging a computationally efficient estimation algorithm, the proposed system offers a promising solution for deployment in dynamic industrial environments.

Future work will focus on transitioning from simulation to real-world implementation, addressing challenges such as environmental variability, multipath interference, and dynamic obstacles. Research directions include integrating additional sensors, such as IMUs, LiDAR, and vision-based systems, to enhance localization robustness. Furthermore, the development of adaptive filtering and machine learning-based phase unwrapping techniques will be explored to improve performance under varying operational conditions. The ultimate goal is to establish a scalable, accurate, and reliable localization framework that can be adapted to a wide range of industrial and service robot applications.

Author Contributions: Conceptualization, T.C.V., M.T.N., and V.T.H.; methodology, M.D.N., L.Q.D., and V.T.H..; software, D.T.N. and M.D.N.; validation, T.C.V., D.T.N., and M.T.N.; formal analysis, M.D.N. and L.Q.D.; investigation, V.Q.T., D.T.N. and M.T.N.; resources, M.D.N.; data curation, T.C.V., L.Q.D.; writing—original draft preparation, D.T.N. and M.T.N.; writing—review and editing, M.T.N., V.Q.T. and S.Q.T.; visualization,; supervision, M.T.N.; project administration, T.V.N. and T.C.V.; funding acquisition, T.V.N. All authors have read and agreed to the published version of the manuscript

Funding: This research received no external funding.

Data Availability Statement: Data can be provided upon request.

Acknowledgments: The authors would like to thank Thai Nguyen University of Technology, Viet Nam (Project T2025-NCS11)

Conflicts of Interest: There is no conflict of interest in this work

References

[1] C. Li *et al.*, "ReLoc: Hybrid RSSI-and Phase-based Relative UHF-RFID Tag Localization with COTS Devices," *IEEE Trans. Instrum. Meas.*, pp. 1–1, 2020, doi: 10.1109/TIM.2020.2991564.

[2] A. Tzitzis, A. Raptopoulos Chatzistefanou, T. V. Yioultsis, and A. G. Dimitriou, "A Real-Time Multi-Antenna SAR-Based Method for 3D Localization of RFID Tags by a Moving Robot," *IEEE J. Radio Freq. Identif.*, vol. 5, no. 2, pp. 207–221, Jun. 2021, doi: 10.1109/JRFID.2021.3070409.

[3] A. Coboi, M. D. M. T. Nguyen, V. N. Pham, T. C. Vu, M. D. M. T. Nguyen, and D. T. Nguyen, "Zigbee Based Mobile Sensing for Wireless Sensor Networks," *Comput. Networks Commun.*, Dec. 2023, doi: 10.37256/cnc.1220233923.

[4] S. Li, M. Hedley, K. Bengston, D. Humphrey, M. Johnson, and W. Ni, "Passive Localization of Standard WiFi Devices," *IEEE Syst. J.*, vol. 13, no. 4, pp. 3929–3932, Dec. 2019, doi: 10.1109/JSYST.2019.2903278.

[5] M. T. Nguyen, L. H. Truong, T. T. Tran, and C.-F. Chien, "Artificial intelligence based data processing algorithm for video surveillance to empower industry 3.5," *Comput. Ind. Eng.*, vol. 148, p. 106671, Oct. 2020, doi: 10.1016/j.cie.2020.106671.

[6] M. T. Nguyen, "An energy-efficient framework for multimedia data routing in Internet of Things (IoTs)," *EAI Endorsed Trans. Ind. Networks Intell. Syst.*, vol. 6, no. 19, p. 159120, Jun. 2019, doi: 10.4108/eai.13-6-2019.159120.

[7] J. A. del Peral-Rosado, R. Raulefs, J. A. Lopez-Salcedo, and G. Seco-Granados, "Survey of Cellular Mobile Radio Localization Methods: From 1G to 5G," *IEEE Commun. Surv. Tutorials*, vol. 20, no. 2, pp. 1124–1148, 2018, doi: 10.1109/COMST.2017.2785181.

[8] A. Mittal, S. Tiku, and S. Pasricha, "Adapting Convolutional Neural Networks for Indoor Localization with Smart Mobile Devices," in *Proceedings of the 2018 Great Lakes Symposium on VLSI*, May 2018, pp. 117–122. doi: 10.1145/3194554.3194594.

[9] A. Parr, R. Miesen, and M. Vossiek, "Comparison of Phase-Based 3D Near-Field Source Localization Techniques for UHF RFID," *Sensors*, vol. 16, no. 7, p. 978, Jun. 2016, doi: 10.3390/s16070978.

[10] X. Teng, Z. Shen, L. Huang, H. Li, and W. Li, "Multi-sensor fusion based wheeled robot research on indoor positioning method," *Results Eng.*, vol. 22, p. 102268, Jun. 2024, doi: 10.1016/j.rineng.2024.102268.

[11] J. Wang and Y. Takahashi, "SLAM Method Based on Independent Particle Filters for Landmark Mapping and Localization for Mobile Robot Based on HF-band RFID System," *J. Intell. Robot. Syst.*, vol. 92, no. 3–4, pp. 413–433, Dec. 2018, doi: 10.1007/s10846-017-0701-8.

[12] M. Hasani, J. Talvitie, L. Sydanheimo, E.-S. Lohan, and L. Ukkonen, "Hybrid WLAN-RFID Indoor Localization Solution Utilizing Textile Tag," *IEEE Antennas Wirel. Propag. Lett.*, vol. 14, pp. 1358–1361, 2015, doi: 10.1109/LAWP.2015.2406951.

[13] C. Wu, Z. Gong, B. Tao, K. Tan, Z. Gu, and Z.-P. Yin, "RF-SLAM: UHF-RFID Based Simultaneous Tags Mapping and Robot Localization Algorithm for Smart Warehouse Position Service," *IEEE Trans. Ind. Informatics*, vol. 19, no. 12, pp. 11765–11775, Dec. 2023, doi: 10.1109/TII.2023.3252405.

[14] K. Srinivasan and J. Gu, "Multiple Sensor Fusion in Mobile Robot Localization," in *2007 Canadian Conference on Electrical and Computer Engineering*, 2007, pp. 1207–1210. doi: 10.1109/CCECE.2007.308.

[15] B. Tao, H. Wu, Z. Gong, Z. Yin, and H. Ding, "An RFID-Based Mobile Robot Localization Method Combining Phase Difference and Readability," *IEEE Trans. Autom. Sci. Eng.*, vol. 18, no. 3, pp. 1406–1416, Jul. 2021, doi: 10.1109/TASE.2020.3006724.

[16] M. T. Nguyen and K. A. Teague, "Compressive and cooperative sensing in distributed mobile sensor networks," in *MILCOM 2015 - 2015 IEEE Military Communications Conference*, Oct. 2015, pp. 1033–1038. doi: 10.1109/MILCOM.2015.7357581.

[17] M. T. Nguyen and K. A. Teague, "Compressive sensing based random walk routing in wireless sensor networks," *Ad Hoc Networks*, vol. 54, pp. 99–110, Jan. 2017, doi: 10.1016/j.adhoc.2016.10.009.

[18] S. Ahuja and P. Potti, "An Introduction to RFID Technology," *Commun. Netw.*, vol. 02, no. 03, pp. 183–186, 2010, doi: 10.4236/cn.2010.23026.

[19] M. T. Nguyen, "Data collection algorithms in wireless sensor networks employing compressive sensing," Oklahoma State University, 2015.

[20] C. Li, L. Mo, and D. Zhang, "Review on UHF RFID Localization Methods," *IEEE J. Radio Freq. Identif.*, vol. 3, no. 4, pp. 205–215, Dec. 2019, doi: 10.1109/JRFID.2019.2924346.

[21] A. Motroni, A. Buffi, and P. Nepa, "A Survey on Indoor Vehicle Localization Through RFID Technology," *IEEE Access*, vol. 9, pp. 17921–17942, 2021, doi: 10.1109/ACCESS.2021.3052316.

[22] C. Chen, Y. Wang, Y. Zhang, and Y. Zhai, "Indoor Positioning Algorithm Based on Nonlinear PLS Integrated With RVM," *IEEE Sens. J.*, vol. 18, no. 2, pp. 660–668, Jan. 2018, doi: 10.1109/JSEN.2017.2772798.

[23] A. Motroni, F. Bernardini, A. Buffi, P. Nepa, and B. Tellini, "A UHF-RFID Multi-Antenna Sensor Fusion Enables Item and Robot Localization," *IEEE J. Radio Freq. Identif.*, vol. 6, pp. 456–466, 2022, doi: 10.1109/JRFID.2022.3166354.

[24] A. M. Whitney, J. M. Parker, Z. C. N. Kratzer, J. T. Fessler, and J. G. Whitney, "Reducing RF Distance Error by Characterizing Multipath," *IEEE Trans. Instrum. Meas.*, vol. 68, no. 9, pp. 3329–3338, Sep. 2019, doi: 10.1109/TIM.2018.2875899.

[25] H. Xu, Y. Ding, P. Li, R. Wang, and Y. Li, "An RFID Indoor Positioning Algorithm Based on Bayesian Probability and K-Nearest Neighbor," *Sensors*, vol. 17, no. 8, p. 1806, Aug. 2017, doi: 10.3390/s17081806.

[26] X. Guo, N. R. Elikplim, N. Ansari, L. Li, and L. Wang, "Robust WiFi Localization by Fusing Derivative Fingerprints of RSS and Multiple Classifiers," *IEEE Trans. Ind. Informatics*, vol. 16, no. 5, pp. 3177–3186, May 2020, doi: 10.1109/TII.2019.2910664.

[27] L. Li, X. Guo, N. Ansari, and H. Li, "A Hybrid Fingerprint Quality Evaluation Model for WiFi Localization," *IEEE Internet Things J.*, vol. 6, no. 6, pp. 9829–9840, Dec. 2019, doi: 10.1109/JIOT.2019.2932464.

[28] F. Martinelli, "A Robot Localization System Combining RSSI and Phase Shift in UHF-RFID Signals," *IEEE Trans. Control Syst. Technol.*, vol. 23, no. 5, pp. 1782–1796, Sep. 2015, doi: 10.1109/TCST.2014.2386777.

[29] M. D. Nguyen and T. T. Nguyen, "Solutions to Improve Indoor Positioning Accuracy supporting Autonomous Mobile Robots," *J. Futur. Artif. Intell. Technol.*, vol. 2, no. 1, pp. 63–78, Apr. 2025, doi: 10.62411/faith.3048-3719-86.

[30] J. Zhang *et al.*, "Toward Robust RFID Localization via Mobile Robot," *IEEE/ACM Trans. Netw.*, vol. 32, no. 4, pp. 2904–2919, Aug. 2024, doi: 10.1109/TNET.2024.3373770.

[31] D. Xie, X. Wang, A. Tang, and H. Zhu, "A Portable RFID Localization Approach for Mobile Robots," *IEEE Internet Things J.*, vol. 9, no. 23, pp. 23332–23347, Dec. 2022, doi: 10.1109/JIOT.2022.3202136.

[32] H. Belaidi and F. Demim, "NURBs Based Multi-robots Path Planning with Obstacle Avoidance," *J. Comput. Theor. Appl.*, vol. 1, no. 4, pp. 478–491, May 2024, doi: 10.62411/jcta.10387.

[33] H. T. Tran *et al.*, "Extended Kalman Filter (EKF) Based Localization Algorithms for Mobile Robots Utilizing Vision and Odometry," in *2022 IEEE 21st Mediterranean Electrotechnical Conference (MELECON)*, Jun. 2022, pp. 91–96. doi: 10.1109/MELECON53508.2022.9843066.

[34] M. T. Nguyen, H. M. La, and K. A. Teague, "Collaborative and Compressed Mobile Sensing for Data Collection in Distributed Robotic Networks," *IEEE Trans. Control Netw. Syst.*, vol. 5, no. 4, pp. 1729–1740, Dec. 2018, doi: 10.1109/TCNS.2017.2754364.

[35] S. Su *et al.*, "Positioning Accuracy Improvement of Automated Guided Vehicles Based on a Novel Magnetic Tracking Approach," *IEEE Intell. Transp. Syst. Mag.*, vol. 12, no. 4, pp. 138–148, 2020, doi: 10.1109/MITS.2018.2880269.